**Science Journal of Chemistry**
2018; 6(4): 66-76
http://www.sciencepublishinggroup.com/j/sjc
doi: 10.11648/j.sjc.20180604.15
ISSN: 2330-0981 (Print); ISSN: 2330-099X (Online)

# Oxidation State of $^{229}$Th Recoils Implanted into $MgF_2$ Crystals

**Beau J. Barker[1, *], Edmund R. Meyer[2], Michael H. Schacht[2], Lee A. Collins[2], Marianne P. Wilkerson[2], Jason K. Ellis[2], Richard L. Martin[2], Xinxin Zhao[2]**

[1]Idaho National Laboratory, Idaho Falls, USA

[2]Los Alamos National Laboratory, Los Alamos, USA

## Email address:

beau.barker@inl.gov (B. J. Barker)

[*]Corresponding author

## To cite this article:

Beau J. Barker, Edmund R. Meyer, Michael H. Schacht, Lee A. Collins, Marianne P. Wilkerson, Jason K. Ellis, Richard L. Martin, Xinxin Zhao. Oxidation State of $^{229}$Th Recoils Implanted into $MgF_2$ Crystals. *Science Journal of Chemistry*. Vol. 6, No. 4, 2018, pp. 66-76.
doi: 10.11648/j.sjc.20180604.15

**Received**: August 31, 2018; **Accepted**: September 25, 2018; **Published**: October 31, 2018

**Abstract:** A solid-state nuclear clock based on the low-lying isomeric state in $^{229}$Th has attracted growing interest. One potential problem for the solid-state nuclear clock approach is the suitability of the doped environment for photon emission of the nuclear isomeric state. Specifically, $Th^{n+}$ $n < 4$ ions could open non-radiative decay routes for deexcitation, hindering the photon emission. Here we have used time-resolved photoluminescence (TRPL) and density functional theory (DFT) calculations to characterize $MgF_2$ crystals that have been implanted with $^{229}$Th recoils via α-decay from a $^{233}$U source with the goal of determining the charge state of the implanted thorium atoms. The DFT calculations predicted $Th^{4+}$ to be the lowest energy oxidation state with $Th^{3+}$ the next lowest in the $MgF_2$ crystal environment. The DFT calculations also show $Th^{4+}$:$MgF_2$ system has a band gap large enough so that the internal electron conversion decay channel is suppressed. Experimentally, we found no evidence for thorium in oxidations state other than +4 using TRPL spectroscopy that has a detection limit for $Th^{n+}$ $n < 4$ ions several orders of magnitude smaller than the number of implanted $^{229}$Th recoils. This work shows that the solid-state approach is a viable option for a nuclear clock.

**Keywords:** $^{229}$Th Isomeric State, Nuclear Clock, Optical Spectroscopy, Density Functional Theory, Thorium Doped $MgF_2$ Crystal

## 1. Introduction

The $^{229}$Th nucleus has an extremely low-lying excited nuclear (isomeric) state [1, 2]. This energy is within the range of current laser technology, making direct excitation of the isomeric state possible and could lead to a new type of nuclear clock with a predicted quality factor of $Q = f/\Delta f \approx 10^{19}$ easily outperforming the current state-of-the-art atomic clocks [3-5]. Such a clock could have a number of applications, such as the potential to test temporal variations of fundamental constants [6, 7], the realization of a γ-ray laser [8], and the possibility of more accurate navigation systems. Precise direct measurement of this transition has proven elusive despite efforts over the past several decades, and a number of groups worldwide are currently engaged in attempts to directly observe and measure deexcitation of this isomeric state [9]. The current, widely accepted value for the transition energy is 7.8 ± 0.5 eV derived from the calorimetric measurement of $^{229}$Th γ-ray emission following the α-decay of $^{233}$U, but the isomer emission was not directly observed in this study [10, 11]. But a recent gas phase study by Wense *et al.* was able to directly observe the deexcitation of the isomeric state, but not accurately measure its energy [12].

Of particular interest is the fact that this isomer could form the basis of a highly accurate solid-state optical frequency reference [4, 13-15]. A solid-state clock is made possible by the fact that the atomic nucleus is shielded from the environment by its electrons, allowing the isomeric transition to keep its narrow line-width even when $^{229}$Th is doped into a crystal. Such a clock would be significantly simpler in

construction when compared to the state-of-the-art gas phase atomic clocks and could result in a highly accurate, smaller and more portable clock. The nuclear clock would consist of a laser locked to the frequency of the isomeric transition, and the laser frequency would be precisely measured using an optical frequency comb.

Most of the recent optical spectroscopy search efforts use $^{229}$Th implanted or doped into a crystal [16-19]. One particular concern for a solid-state system is the band gap of the doped material. Isomer deexcitation could occur through internal conversion if the band gap of the doped material is less than the energy of the isomeric state. A theoretical study by Tkalya *et al.* stresses that, if present, non-radiative routes will dominate the deexcitation, quenching any photon emission from the isomeric state [20]. As will be shown below, the oxidation state of the implanted thorium atoms greatly influences the band gap. $Th^{4+}$ is the preferred oxidation state due to the closed shell, radon-like electronic configuration. DFT calculations have predicted that $Th^{4+}$ doped into either $CaF_2$ or $MgF_2$ crystals (see Section II, Theory for results on the $Th^{4+}$:$MgF_2$ system) only slightly affects the band gap of these materials. Thorium in lower charge states has valence electrons and consequently has low-lying electronically excited states that could have a significant effect on the band gap of the doped material. While thorium is typically found as $Th^{4+}$ in condensed phases, the presence of thorium in other oxidation states is quite rare [21], it is not known for certain what the chemical environment of the thorium ions is in the solid-state studies conducted so far. The failure to detect emission from the isomeric state in the previous studies could be due to an unsuitable chemical environment, lattice defect sites or impurities could cause the thorium ions to be in lower-valence states or in unsuitable chemical forms [22].

For thorium atoms implanted into $MgF_2$ plates the most likely charge state is 4+, but the implantation process, via radioactive decay, is a violent non-equilibrium one and any resulting defects in the crystal may result in $Th^{n+}$ ions in charge states less than 4+ in the lattice. This leaves open the possibility that a significant portion of the thorium ions are in lower valence states. Further complicating the matter are studies conducted with the MLL buffer-gas stopping cell characterizing the α-decay recoils from a $^{233}$U source [12, 23, 24]. These studies have shown that a significant portion of the $^{229}$Th recoils are emitted in charge states less than +4. Thus, the thorium atoms have the potential to implant in lower oxidation states.

Given the importance of eliminating potential non-radiative deexcitation channels, we have undertaken a spectroscopic and theoretical study of $MgF_2$ plates that have been implanted with $^{229}$Th recoils following α-decay of a $^{233}$U source. This study focuses on detecting the presence of $Th^{n+}$ ions, where $n < 4$, in these plates. It should be noted that $Th^{4+}$ does not luminesce because it is closed shell; it has no low-lying electronically excited states. Similar optical plates are currently in use at Los Alamos National Laboratory (LANL) to directly observe photon emission from the isomeric state [16]. We employed time-resolved photoluminescence (TRPL), γ-ray spectroscopy and DFT calculations to characterize the implanted plates. Because we detected no signal from thorium ions in charge states less than 4+ we analyzed the detection limit of our apparatus to provide an upper estimate for the number of such ions possible in the plates.

# 2. Theoretical Results

We performed density functional theory (DFT) calculations on thorium doped $MgF_2$ crystals using the *Vienna ab initio Simulation Package* (VASP) suite of software [25-28]. The local density approximation (LDA) [29] was used with an energy cutoff of 400 eV and a 4x4x4 Γ-centered k-point grid was chosen to sample the momentum space. Geometry optimizations were performed such that the forces were converged to 0.01 eV/Å, and the energies to $10^{-6}$ eV. A similar set of calculations was recently performed in $CaF_2$ [30]. In all, four separate systems were chosen to study the possible ways in which thorium atoms might embed in a host $MgF_2$ crystal. Typically, one uses crystal chemistry formulations where fluoride complexes of each species are added together, reacted, and new doped species emerge. For example, to get Th in the +4 oxidation in the crystal we would write:

$$(MgF_2)_n + ThF_4 + \Delta E^{c\prime}_{4+} \rightarrow Th^{4+}F_4{:}(MgF_2)_{n-1} + MgF_2. \quad (1a)$$

However, in an experiment where we bombard an $MgF_2$ crystal with $^{229}$Th recoils via the radioactive decay of $^{233}$U atoms, it might be more apt to use the atomic formalism:

$$(MgF_2)_n + Th + 2F + \Delta E^{a\prime}_{4+} \rightarrow Th^{4+}F_4{:}(MgF_2)_{n-1} + Mg. \quad (1b)$$

In the above, Th, Mg, or F is the chemical potential of the element at standard temperature and pressure. In the case of Th and Mg we use the crystal geometries of these species while in the case of F, we use the diatomic gas state. Likewise, $ThF_4$ would be the chemical potential for the single crystal unit of that substance. The difference in the approaches lies in the zeroes of energy. Each approach will lead to a different value for $\Delta E$. The other reactions we studied are given by:

$$(MgF_2)_n + ThF_4 + \Delta E^{c}_{3+} \rightarrow Th^{3+}F_3{:}(MgF_2)_{n-1} + MgF_2 + F, \quad (2a)$$

$$(MgF_2)_n + Th + F + \Delta E^{a}_{3+} \rightarrow Th^{3+}F_3{:}(MgF_2)_{n-1} + Mg, \quad (2b)$$

$$(MgF_2)_n + ThF_4 + \Delta E^{c}_{2+} \rightarrow Th^{2+}F_2{:}(MgF_2)_{n-1} + MgF_2 + 2F, \quad (3a)$$

$$(MgF_2)_n + Th + \Delta E^{a}_{2+} \rightarrow Th^{2+}F_2{:}(MgF_2)_{n-1} + Mg, \quad (3b)$$

$$(MgF_2)_n + ThF_4 + \Delta E^{c''}_{4+} \rightarrow Th^{4+}F_4{:}(MgF_2)_{n-2} + 2MgF_2, \quad (4a)$$

$$(MgF_2)_n + Th + \Delta E^{a''}_{4+} \rightarrow Th^{4+}F_4{:}(MgF_2)_{n-2} + 2Mg. \quad (4b)$$

In the above equations, a) and b) stand for crystal reference and atomic reference energies respectively. We studied Th substituting for Mg in the +2 oxidation state (2a, b), +3 oxidation state with one F interstitial (3a, b), +4 oxidation state with 2 F interstitials (1a, b), and +4 oxidation state with one Mg vacancy (4a, b). If one grows a doped crystal using fluoride powders, (1a-4a) should be used. When performing an experiment with Th atoms by ballistically bombarding the surface of a crystal, (1b-4b) are more appropriate.

The chemical potentials are calculated in the following way for each species. In the cases of Th and Mg, we use the metal geometries associated with each atom and reduce it to a single atomic energy. This ensures that we incorporate the effects of vibrations into the chemical potential. In the case of F, we use the gas phase of $F_2$ molecules for which a large, asymmetric box was used to calculate the energy of the diatom. Crystals of $ThF_4$ and $MgF_2$ were optimized with similar k-point meshes and plane wave cutoff energies as the doped systems and the chemical potential extracted for the single crystal unit. All values are extracted for the zero-temperature limit where the free energies can be associated with the chemical potential.

***Table 1.*** *Formation energies for $Th^{2-4+}$ doped $MgF_2$ crystals.*

| Energy | Crystal Reference (eV) | Atomic Reference (eV) |
|---|---|---|
| $\Delta E_{2+}$ | 16.1 | 5.6 |
| $\Delta E_{3+}$ (x, y) | 9.9 | -0.6 |
| $\Delta E_{3+}$ (z) | 13.4 | 2.9 |
| $\Delta E'_{4+}$ | 4.6 | -5.9 |
| $\Delta E''_{4+}$ | 2.1 | 3.1 |

The values for the formation energies for a *2x2x2* supercell of $MgF_2$, which results in *n=16,* are reported in Table 1. In Table 1, $\Delta E_{n+}$ stands for thorium in the $n^+$ oxidation state. For the $Th^{3+}$:$MgF_2$ system two geometries were considered; one where the F interstitial is placed in the planar direction, denoted as $\Delta E_{3+}$(x, y), and one along the z-axis denoted as $\Delta E_{3+}$(z). $\Delta E'_{4+}$ and $\Delta E''_{4+}$ are the formation energies for the $Th^{4+}$:$MgF_2$ system for the cases with charge compensation using F interstitial atoms and Mg vacancy respectively. In each case, atomic or crystal reference, the $Th^{4+}$ doped system is the lowest energy system. Interestingly, interstitial F atom formation is preferred for the atomic reference case, while Mg vacancy is the energetically preferred route for the crystal reference case. The two fluorine interstitials could be placed into two possible configurations, linear and bent. Calculations showed these geometries were nearly identical in energy. What we note is the discrepancy in $\Delta E_{4+}$ between the crystal and atomic reference formulations. A discrepancy is expected due to the nature of the chemical offsets introduced. For the crystal reference formulations, the energy of formation is associated with swapping $ThF_4$ with $MgF_2$. This heat of formation is what causes all of the energies in the crystal formulation to be positive. In contrast, the energy of formation is negative for the atomic reference formulations. Here Th atoms are launched at the $MgF_2$ crystal and embedded, the dislodged F atoms are free to partake in the bonding procedure as interstitial atoms, and Th atoms are oxidized from the neutral atom into the more favorable +4 charge state. This process is predicted to give off about 5.9 eV of energy.

Thorium in the 3+ oxidation state is the next highest in the energy for the atomic and crystal reference cases. As stated above the interstitial F atom can be placed along the planar (x or y) direction, or along the z-axis. The lower energy solution is found to be planar. Placing the F atom along the z-axis was 3.5 eV higher in energy. For the atomic reference case, the reaction was predicted to be favorable by 0.6 eV. Lastly, calculations for $Th^{2+}$ imbedded into the crystal were predicted to be the highest in energy.

We performed calculations using the $G_0W_0$ approximation [31, 32] within the VASP code to calculate the band gap of the undoped and the $Th^{4+}$ and $Th^{3+}$ doped $MgF_2$ materials. The $G_0W_0$ approximation is a many-body Green's function approach that generally gives reasonable results for wide-gap semi-conductors. [33] We used 512 (544) bands and a 4x4x4 k-point Γ-centered mesh in the calculation of the optical properties of the undoped (doped) system. We also calculated the band structure which was generated using the Wannier90 software, the input files of which are integrated with the output of VASP [34].

Our calculated band gap for the undoped $MgF_2$ system is 12.5 eV, in good agreement with the experimental value of 12.4 eV [35, 36]. For the system with $Th^{4+}$ doped into the $MgF_2$ crystal, having two fluorine interstitials, we found an indirect Z-A band gap of 11.6 eV. The density-of-states (DOS) for this system is shown in Figure 1. The 4f and 5d electrons are in the lower part of the Mg valence band while the interstitial fluorine atoms are raised slightly in the conduction band leading to an overall decrease in the band gap. However, the total gap remains wide enough to encompass the expected isomeric transition in the $^{229m}$Th decay, and therefore the internal conversion channel is closed.

In the case of Th in the +4 oxidation state with an associated Mg vacancy near the Th site, we find a band gap of 11.9 eV. In this scenario, which can happen in the case of $MgF_2$ crystals grown with $ThF_4$ powders at elevated temperatures, the conduction band is once again raised relative to the Mg valence band causing a decrease in the

overall band gap. However, the d and f electrons of the Th atom are well into the Mg valence band as can be seen on the right-hand side of Figure 2. The general structure of the Mg valence band is preserved and role of the Th atom is to break some of the symmetries in the path. We find that the band gap transition remains a direct Γ-Γ transition. Again, the total band gap is large enough to suppress the internal conversion channel.

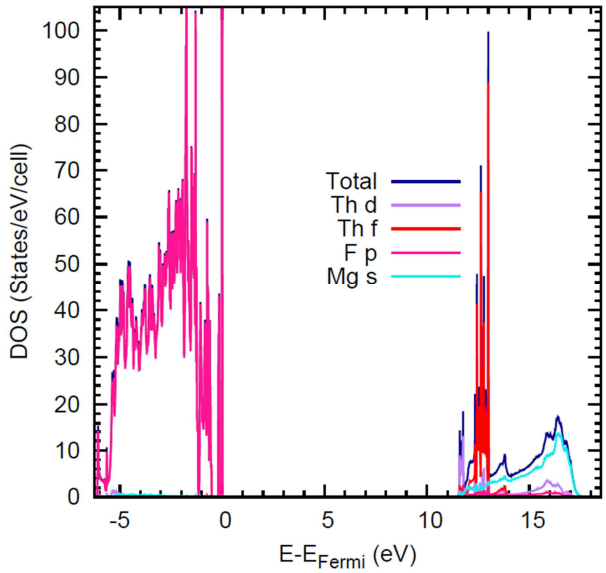


***Figure 1.*** *Density of states for the $Th^{4+}$:$MgF_2$ doped crystal with two F interstitial atoms.*

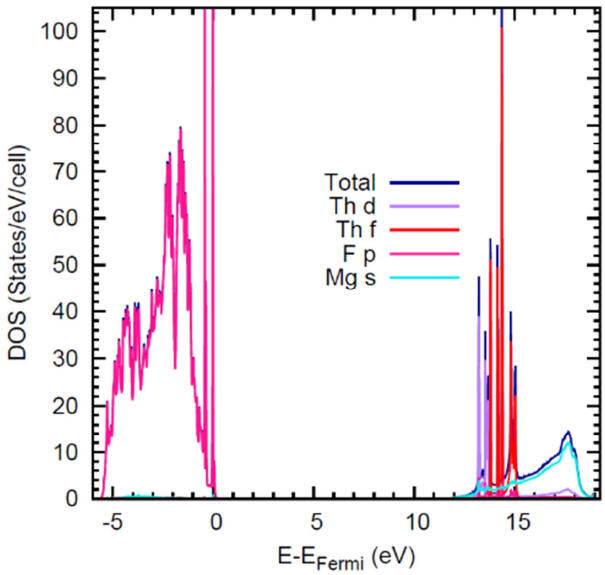


***Figure 2.*** *Density of states for the $Th^{4+}$:$MgF_2$ doped crystal with the Mg vacancy.*

The next candidate for observation is the +3 oxidation state, which due to the implantation process may exist in the crystal leading to a diminishing of the photon signal form the isomeric state if an internal conversion pathway is opened. To study this system we again used a spin-polarized $G_0W_0$ calculation, 512 bands, and a 4x4x4 Γ-centered k-mesh. Due to the increased computational effort of the spin-polarized calculation, we had to decrease the number of bands in order to meet our computational restrictions. The results of the spin-polarized calculation are presented in Figure 3. The upper and lower panels are the α- and β-spins, respectively. We find that the α-band-gap is about 1.0 eV (1240 nm), much too small to suppress internal conversion and therefore could allow the process to occur. The β-band-gap is about 11.0 eV. The α-gap is indirect R-A transition. The highest occupied β-bands are interstitial fluorine bands that are well localized due to their flat nature in k-space. The highest occupied α-band is a d-orbital on the thorium-site. We found that this non-localized band has a correspondingly small DOS associated with it and that the peak is more pronounced in the lower portion of the band near the Γ-point. While the gap to the lowest unoccupied band is about 1eV, it is of an indirect nature. The lowest unoccupied band is given by f-orbitals on the thorium atom. These orbitals, while more localized, are spread out in energy in the DOS. The strongest transition is a direct transition along the Γ-path which is around 3eV.

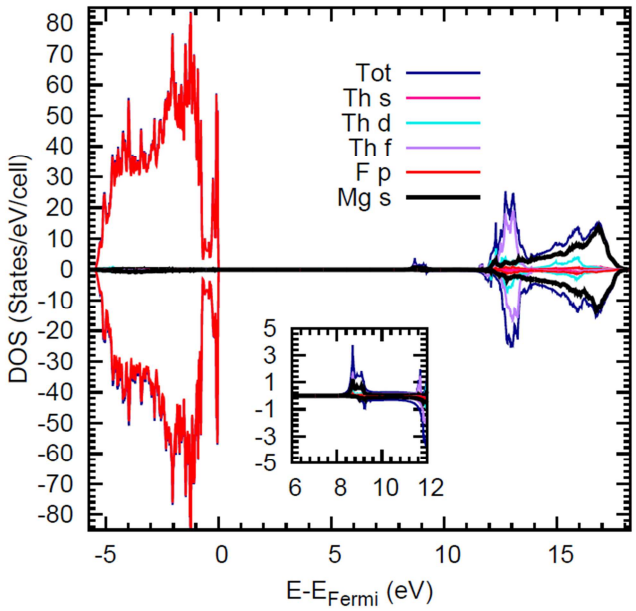


***Figure 3.*** *Density of states for the $Th^{3+}$:$MgF_2$ crystal with one F interstitial along with x-axis. The upward trace represents the α-spins the downward trace the β-spins.*

## 3. Experimental Methods

The $^{229}$Th ($t_{1/2}$ = 7917 years [37]) implanted plates were created by exposing square $MgF_2$ plates (2 x 2 x 0.1 cm Almaz Optics) to a $^{233}$U source, which contained an 8 ppm $^{232}$U impurity. $^{233}$U ($t_{1/2}$ = 159, 200 years) decays by emitting an α-particle resulting in $^{229}$Th recoils with ~83 keV of kinetic energy. The $^{233}$U source is composed of two 2 cm diameter gold plated stainless steel disks which were electrodeposited with 17 μg/cm$^2$ of a $^{233}UO_2$ film. The $^{233}$U source disks were placed on either side of the $MgF_2$ plates for about 2500 hours. To rule out emission from color centers or

impurities in the $MgF_2$ plates, control plates were created by inserting an aluminized Mylar foil (2.2 μm thick) between the $^{233}U$ source and the $MgF_2$ plates. This allowed the α-particles to implant into the plates while blocking the lower-energy $^{229}Th$ recoils.

The spectrometer used in this study has been described in detail previously [38, 39]. Briefly, the excitation source is a Nd:YAG pumped (Continuum Surelite II) optical parametric oscillator (OPO, Continuum Panther) operating at a repetition rate of 10 Hz; the OPO has a spectral band width of 5 $cm^{-1}$ and a temporal width of about 8 ns. The laser's energy was not attenuated prior to interaction with the sample and the energy of each pulse was typically about 5 mJ. Emission was collected at 90° relative to the excitation laser. Luminescence was dispersed through a 300 mm monochromator (Action Research Corporation Spectra Pro 300i), passed through a 650 nm long pass filter and imaged onto an InP/InGaAs PMT (Hamamatsu R5509-72). The PMT is sensitive between 300 and 1700 nm. The signal from the PMT was amplified and sent either to a photon counter (Stanford Research SR-400) for luminescence spectra or to a multichannel scaler/averager (Standford Research SR-430) to collect time-resolved luminescence decay curves. Both of these have a response time of 10 ns. All spectra presented here were recorded using 0.75 - 1.0 mm slit width. Time-resolved single photon counting was used to collect luminescence spectra. Here all signal and noise events are counted within a certain time after the excitation pulse. Using time-gating has the advantage that noise events after the luminescence has decayed can be ignored.

The γ-ray spectrum was recorded in "The Nuclear and Radiochemistry Radionuclide Assay Facility" at LANL using a high purity germanium detector with a resolution of 2 keV. The γ-rays from the $MgF_2$ plates were counted for 3000 min. The identities of peaks and their branching ratios were determined using the known energy lines from the "WWW Table of Radioactive Isotopes" database [40]. The total number of counts was derived by fitting Gaussian functions to features in the spectrum and using the analysis program Specanal. The energy scale was calibrated and the number of photon counts has been corrected for the efficiency and geometry of the detector.

# 4. Experimental Results

### *4.1. Luminescence Spectra*

For our spectroscopic measurements, we collected time-resolved photoluminescence (TRPL) spectra from three types of $MgF_2$ plates: those exposed to $^{229}Th$ recoils and α-particles, those exposed to only α-particles and unexposed $MgF_2$ plates. The control plates were used to distinguish emission from color centers and impurities present in the plates, or emission from optical components in the detection system from that potentially belonging to thorium ions. Spectra were collected before and after annealing the plates to 250° C and using two different time-gates after the excitation pulse.

In order to obtain spectra with the best signal-to-noise ratio (S/N) for the TRPL spectra, time-resolved luminescence decay curves were recorded. This was done in order to choose an optimum time-gate ie. one which is long enough to capture the luminescence after the excitation pulse, but short enough to exclude noise events which occur after the luminescence has decayed. A typical time-resolved luminescence decay curve is shown in Figure 4. The curve was similar for all three plates after annealing, and for a variety of excitation and emission wavelengths. Luminescence was monitored out to 6 μs after the pump pulse. The luminescence decay curve in Figure 4 was recorded using the annealed $^{229}Th$ implanted plate with an excitation wavelength of 550 nm while monitoring emission at 1050 nm. Also shown in Figure 4 is the temporal profile of the laser pulse. The curve in Figure 4 shows a fast decay visible just after the portion of the curve belonging to the excitation pulse. Fitting a single exponential decay function to this portion of the decay curve gives a lifetime of ~25 ns. Because emission was only observed within the first 150 ns after the excitation pulse, TRPL spectra were recorded using two time-gates: one from t = 0 to 350 ns and a second one from t = 50 to 350 ns after the excitation pulse. The second gate was used to record TRPL spectra in order to exclude the emission taking place during the excitation pulse. The TRPL spectra presented below were recorded using the t = 0 to 350 ns gate unless otherwise specified.

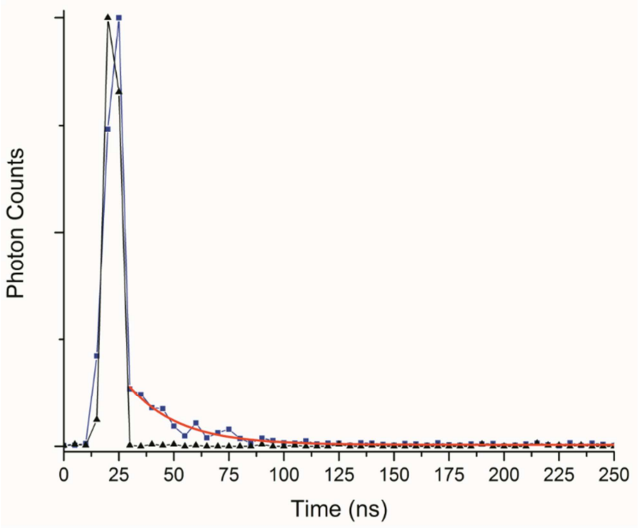


***Figure 4.*** *Time-resolved luminescence decay curve for the $^{229}Th$ implanted $MgF_2$ plate after annealing. The trace represented by squares was recorded while monitoring emission at 1050 nm following paused excitation at 550 nm, and the trace represented by triangles is the decay profile of the excitation laser. The solid line is a fit using a single exponential decay function.*

Initially, we measured TRPL spectra from unexposed $MgF_2$ plates. Emission from the unexposed plates was monitored after pulsed excitation at 415 nm, 575 nm and 610 nm. The TRPL spectrum of these plates shows two broad features from about 650-900 nm and 1250-1650 nm for

excitation at 575 nm and 610 nm. Excitation at 415 nm results in much weaker emission lacking the features observed for 575 nm and 610 nm excitation. We hypothesized that some of the features observed in the TRPL spectra were due to emission from color centers. We attempted to eliminate the color center emission by annealing the plates in an oven at 250°C for one week. Figure 5 shows TRPL spectra of the unexposed plates after annealing, and the spectra are nearly identical for all three excitation wavelengths. The spectra recorded using 575 nm and 610 nm excitation show a dramatic change in both the structure and intensity of emission while the spectra recorded using 415 nm excitation is largely unchanged. TRPL spectra were also recorded after an additional seven days of annealing, and no significant changes were detected. As can be seen in Figure 5, some emission remains from the plates even after annealing. This emission could be from a number of sources, such as impurities in the plates or other color centers, which were not removed by the annealing process. The "step" feature at about 1300 nm could be due to 2$^{nd}$ order diffraction belonging to features starting at about 650 nm or to emission belonging to the long pass filter itself. Emission spectra collected using different long pass filters also showed a similar "step" feature at wavelengths which would correspond to 2$^{nd}$ order diffraction, i.e. when a 600 nm long pass filter was used the "step" feature shifted to 1200 nm.

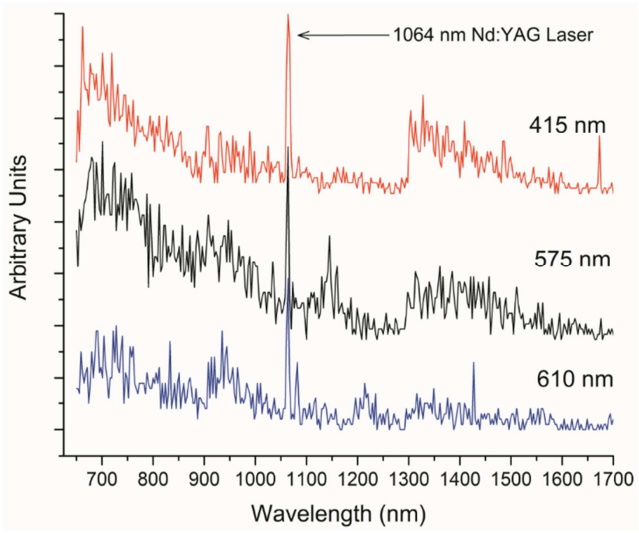


***Figure 5.*** *Time-resolved photoluminescence spectra for the pure $MgF_2$ plates after annealing at 250°C using excitation wavelengths: 415 nm, 575 nm and 610 nm.*

Before the plates were annealed, we also found evidence for emission from color centers, which were caused by radiation damage. Both the plates implanted with $^{229}$Th recoils and those implanted with only α-particles have a broad relatively intense feature from approximately 900-1200 nm that is not present in the control disk. Because this feature was not observed in the unexposed plates, we hypothesized that it may be due to emission from radiation-induced color centers. Again, we attempted to remove the color centers by annealing the plates and, after annealing, the broad feature largely disappears in both types of plates.

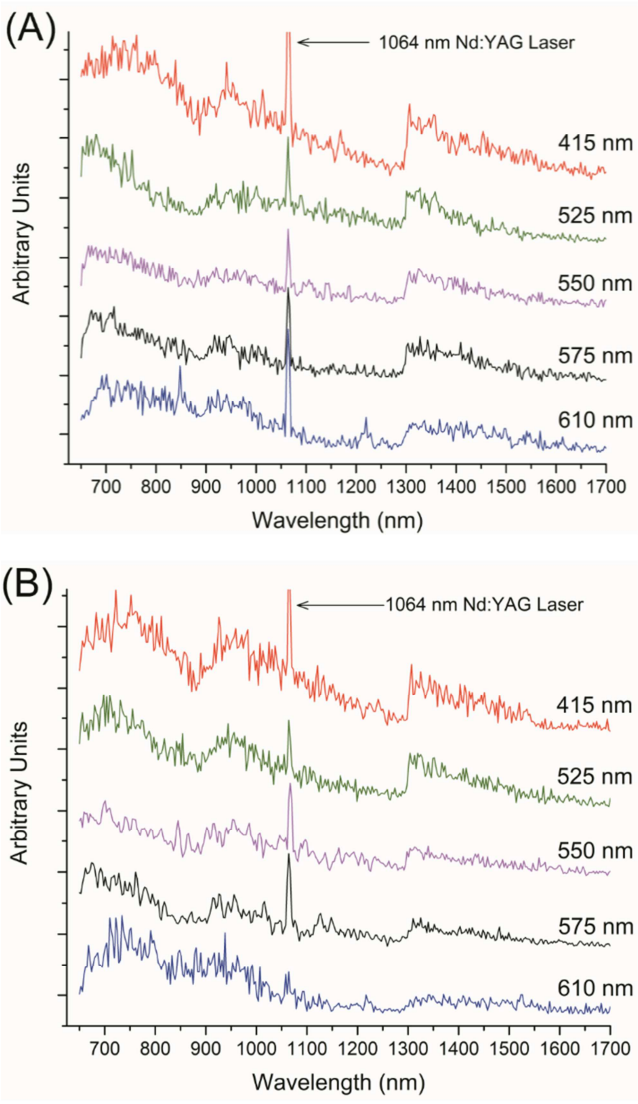


***Figure 6.*** *Time-resolved photoluminescence spectra of the $MgF_2$ plates implanted with $^{229}$Th recoils (A) and only α-particles (B) after annealing at 250°C using excitation wavelengths: 415 nm, 525 nm, 550 nm, 575 nm and 610 nm.*

TRPL spectra of the annealed $^{229}$Th recoil implanted plates and those implanted with only α-particles were recorded using excitation wavelengths: 415 nm, 525 nm, 550 nm, 575 nm and 610 nm. It should be noted that $Th^{4+}$ is closed shell and will not luminescence. Figure 6 shows TRPL spectra of the annealed $^{229}$Th implanted plates and the plates exposed to only α-particles recorded using these excitation wavelengths. Close inspection of Figure 6 shows that the spectra recorded using both types of plates are nearly identical. The exception to this are two small, relatively narrow features centered at approximately 850 nm and 1220 nm. These features are due to a small amount of laser light originating from the idler of the OPO and a second order diffraction peak belonging to the excitation wavelength. We conclude that we cannot detect any emission from $Th^{n+}$ $n < 4$ ions in our implanted crystal over the range of 650-1700 nm. The luminescence spectra

collected using the second time gate (50-350 ns) produced spectra with only features present in Figure 6.

### *4.2. γ-Ray Spectrum*

We recorded a γ-ray spectrum from both the plates implanted with $^{229}$Th recoils and those implanted with only α-particles in order to assess how effective the $^{233}$U source is at implanting the $^{229}$Th recoils. Because the half-life of $^{229}$Th is long (7917 years [37]), we did not expect to detect any features belonging to γ-ray emission from the decay of $^{229}$Th or its daughters above the noise. Instead, we detected γ-ray emission from the decay daughters belonging to $^{228}$Th. This radioisotope has a much shorter half-life of 1.91 years. $^{228}$Th was present in the plates due to a 8 ppm $^{232}$U impurity in the source, which decays by emitting an α-particle to $^{228}$Th. The γ-ray spectrum collected from the $^{229}$Th implanted $MgF_2$ plates is shown on Figure 7. The number of photon counts has been corrected for the geometry and detection efficiency of the spectrometer and the background has been removed. Peaks belonging to all of the $^{228}$Th daughters were detected except for $^{220}$Rn, as expected. A γ-ray spectrum was collected from the plates implanted with only α-particles as well. This spectrum was nearly identical to the background spectrum and confirms that the Mylar sheet blocked the $^{228}$Th and $^{229}$Th recoils from reaching the plates.

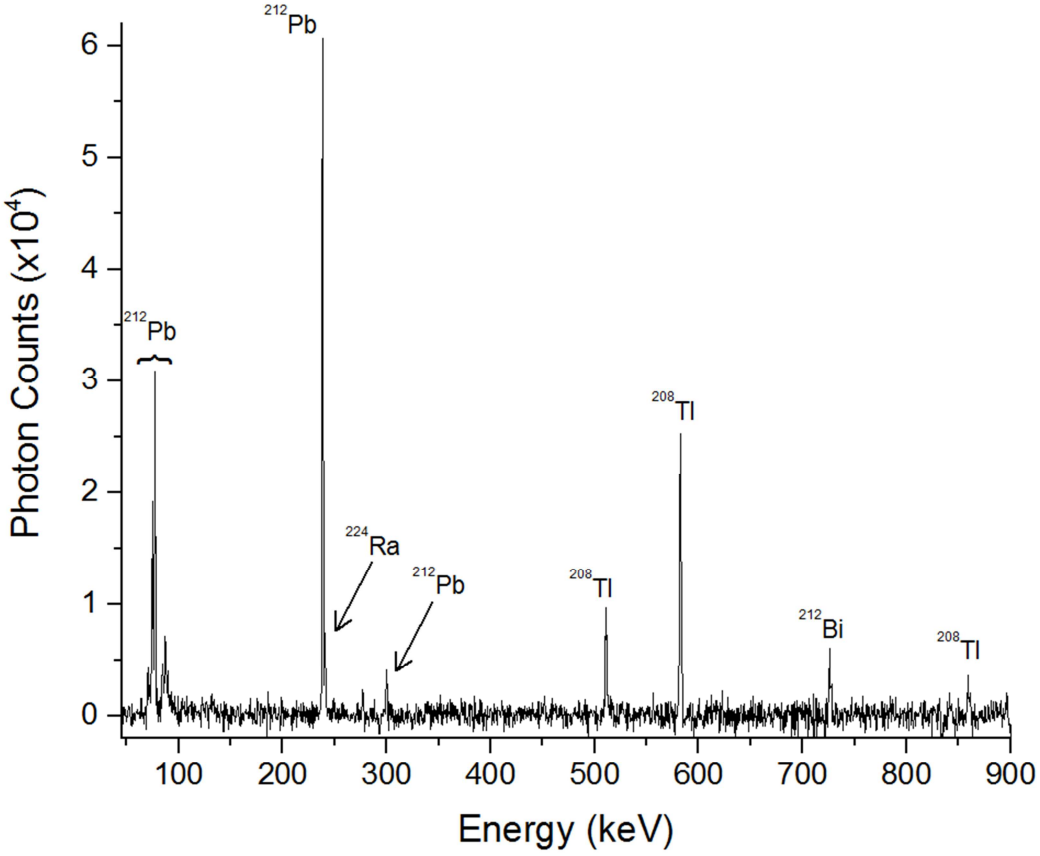


***Figure 7.*** *γ-ray spectrum recorded while monitoring the $MgF_2$ plates implanted with $^{229}$Th recoils.*

To calculate the number of $^{228}$Th implants we assumed the members of its decay chain were in secular equilibrium. This assumption is justified because the age of the plates at the time the γ-ray spectrum was recorded (~1.7 years) is similar to the half-life of $^{228}$Th (1.91 years), allowing an equilibrium to be established, and the decay rate of $^{228}$Th is orders of magnitude slower than any of its daughters. The number of $^{228}$Th atoms implanted into the plate is calculated using (5):

$$N_{228} = \frac{A_d / exp^{-(\lambda_{Th} t_r)}}{I_g * \lambda_{Th}} \quad (5)$$

where $\lambda_{Th}$ is the decay constant of $^{228}$Th, $A_d$ is the activity of a given transition in the γ-ray spectrum, $I_g$ is the branching ratio for that transition, $t_r$ is the time after the plates were removed from the source, and $N_{228}$ is the number of $^{228}$Th atoms present in the disk. Equation 5 gives a lower limit on the number of $^{228}$Th implants. A small number of $^{228}$Th atoms decay during the time the plates were exposed to the source (~2500 hours). A simulation, assuming all $^{228}$Th recoils implant into the plates, shows that including $^{229}$Th recoils which decayed during the implantation time increases the number of $^{229}$Th implants by only about 5%. The number of $^{229}$Th implants is then found by multiplying $N_{228}$ by the ratio of the activities of $^{233}$U to $^{232}$U in the source.

The results from the γ-ray spectrum are shown in Table 2, which contains the isotope, activity, the measured energy, and the branching ratio [40] for each transition observed in the γ-ray spectrum, along with the number of $^{228}$Th and $^{229}$Th

implants, as well as the implantation efficiency. The number of $^{228}$Th and $^{229}$Th recoils in the plates is 3.9 x $10^8$ and 2.2 x $10^{10}$ respectively and implantation efficiency of the $^{233}$U source is 14%.

***Table 2.*** *Results from the $^{229}$Th implanted $MgF_2$ plate γ-ray spectrum.*

| Isotope | Transition (keV) | Activity (Bq) | $I_g$ | $N_{228}$ x $10^8$ | $N_{229}$ x $10^{10}$ | % Implantation |
|---|---|---|---|---|---|---|
| $^{212}$Pb | 74.8 | 0.28 | 0.104 | 4.3 | 2.4 | 15 |
| $^{212}$Pb | 77.1 | 0.40 | 0.175 | 3.7 | 2.1 | 13 |
| $^{212}$Pb | 238.6 | 0.99 | 0.433 | 3.7 | 2.1 | 13 |
| $^{224}$Ra | 241.0 | 0.11 | 0.041 | 4.2 | 2.4 | 15 |
| $^{212}$Pb | 300.1 | 0.09 | 0.030 | 4.8 | 2.7 | 17 |
| $^{208}$Tl | 510.8 | 0.22 | 0.226 | 4.4 | 2.5 | 15 |
| $^{208}$Tl | 583.2 | 0.64 | 0.845 | 3.4 | 1.9 | 12 |
| $^{212}$Bi | 727.3 | 0.14 | 0.066 | 3.4 | 1.9 | 12 |
| $^{208}$Tl | 860.6 | 0.09 | 0.124 | 3.1 | 1.7 | 11 |
| | | | Average | 3.9 | 2.2 | 14 |

# 5. Anaylsis of Detection Limits

We have detected no evidence for $Th^{n+}$ n < 4 ions in the $MgF_2$ plates within the sensitivity of our apparatus. To get an upper estimate on the number of possible luminescent thorium ions in our plates we have estimated the limit-of-detection (LOD) for our apparatus; $Th^{4+}$ ions will not luminescence because they are closed shell and do not possess any low-lying excited electronic states. The number of signal photons collected for a given number of laser shots is shown in (6):

$$N_s = \Phi\eta f_{ex} N_{sh} N_{n+} f_t, \tag{6}$$

where $N_s$ is the total number of signal counts, $\Phi$ is the quantum yield and fraction of the emission spectrum collected by the monochromator, η is the detection efficiency of the apparatus which accounts for the fraction of the plate illuminated by the laser beam, the solid angle of collection and the quantum efficiency of the PMT. The fraction of the ions excited after the laser pulse is $f_{ex}$, $N_{sh}$ is the number of laser shots, $N_{n+}$ is the total number of $Th^{n+}$ ions, where n < 4, present in the $MgF_2$ plate, and $f_t$ is a function to account for the temporal behavior of the excited state ion's decay. In our experiment, typically 300 shots were used to collect each data point in the emission spectrum. The quantum efficiency of the PMT is 1% and the detection efficiency (η) was estimated to be 7.8 x $10^{-6}$. For the quantum yield, we used a value of 1% that we believe to be a conservative estimate based on the predicted band gap of the $Th^{3+}$:$MgF_2$ system (1.0 eV). $Th^{3+}$ is considered here because it is the most likely oxidation state to be present in the implanted plates after $Th^{4+}$, that is it is the next oxidation state in energy after $Th^{4+}$. (See Section II. Theory for details.) The nonradiative relaxation rate is exponentially dependent on the size of the energy gap and the number of phonons required to bridge it. This relationship is known as the "energy gap law." [41, 42] A rule of thumb is that if the number of quanta of the largest vibrational mode present in the molecule is more than six times the energy gap, then deexcitation by emitting a photon is competitive with nonradiative multiphonon processes [42]. In our system, the largest energy vibrations available to couple to are the metal-fluorine vibrational modes. An IR study of $ThF_3$ and $ThF_4$ isolated in an inert gas matrix [43] gives their largest vibrational modes as ~550 $cm^{-1}$, while IR and Raman studies using single crystals of $MgF_2$ gives the largest vibrational mode as 625 $cm^{-1}$ [44, 45]. Using the calculated band gap of 1.0 eV (8065 $cm^{-1}$) and assuming coupling to the largest vibrational mode of $MgF_2$ gives the number of phonons required to bridge the gap as 13. Thus, we believe that deexcitation by radiative emission should be probable. Experimentally there is evidence for low energy gap actinides having relatively high quantum yields. One example is the $U^{3+}$:$CaF_2$ system with an energy gap of about 3830 $cm^{-1}$ (2.613 μm) and formed the basis of the second known laser system [46, 47].

The excited state fraction depends on the relative size of the excitation and decay rates during the pump pulse and is given in (7):

$$f_e = \frac{\gamma_e}{(2\gamma_e+\gamma_d)}\left(1 - exp^{-(2\gamma_e+\gamma_d)t_p}\right), \tag{7}$$

where $\gamma_e$ and $\gamma_d$ are the excitation and decay rates respectively and $t_p$ is the temporal width of the excitation pulse. The size of $\gamma_e$ can be found using (8):

$$\gamma_e = I\sigma. \tag{8}$$

Here $I$ is the intensity of the laser beam and σ is the absorption cross section of the excited electronic state. Typical pulse energies used here are about 5 mJ at 550 nm. The area of the beam is 19.6 $mm^2$ and the temporal width of the laser pulse is 8 ns giving an intensity of 9 x $10^{28}$ photons/($m^2$*s). Typical absorption cross sections for spin and orbitally allowed electronic transitions are on the order of 1.7 x $10^{-22}$ – 8.3 x $10^{-21}$ ($m^2$), for metal containing complexes [47, 48]. The low-energy excited states in the $Th^{3+}$:$MgF_2$ system are allowed d-f type transitions and the DOS above the band gap is rather high, (see Figure 3) which gives us confidence that we will be resonant with an excited electronic state upon excitation. Using these values, excitation rates between 1.5 x $10^7$ and 7.3 x $10^8$ ($s^{-1}$) are obtained. If we assume that the excited state lifetime is on the order of 0.1 μs (corresponding to a decay rate of 1 x $10^7$ ($s^{-1}$)) (7) gives excited state fraction as 50%. Even if the decay rate is an order of magnitude larger, $f_{ex}$ is still 10% for the lower estimate of the absorption cross section. Given the above

considerations, we will assume $f_{ex}$ is 50% for the LOD calculation.

The temporal behavior of the excited state decay is divided into two parts. The first accounts for the emission which occurs during the pump pulse and the second for emission which occurs after the pump pulse. The number of counts for each period is given in (9a) and (9b) where the sum of these two equations is equal to $N_s$,

$$N_{pump} = \Phi\eta f_{ex} N_{sh} N_{n+}(t_p/\tau), \quad (9a)$$

$$N_{decay} = \Phi\eta f_{ex} N_{sh} N_{n+}(1 - exp^{(-t_g/\tau)}). \quad (9b)$$

Where $N_{pump}$ and $N_{decay}$ are the number of counts for each period, again $t_p$ is the temporal width of the pump pulse, $t_g$ is the length of the time-gate after the pump pulse and $\tau$ is the lifetime of the excited electronic state. Equation (9a) assumes that the population of the excited state remains constant over the pump pulse and (9b) assumes that the excited state decays via a single exponential.

Overall, the sensitivity will depend on several factors: the number of background counts collected, the lifetime of the excited state, the size of the counting period and the signal-to-noise (S/N) ratio desired to determine the probability of obtaining a false positive. Longer lifetimes result in lower sensitivity as the photons from the species of interest are more spread out in time. This requires a longer $t_g$ to collect the signal events and so more noise is collected as a result. Lastly, the desired value for the S/N ratio has to be chosen. To estimate the sensitivity of our apparatus we used an S/N=3, as this gives only an ~5% probability of obtaining a false positive.

Assuming Poisson statistics the S/N ratio is given by,

$$S/N = \frac{N_s}{\sqrt{N_s + N_b}}, \quad (10)$$

where $N_b$ is the number of background counts collected. The size of $N_b$ is a function of the number of laser shots and noise rate per unit time (the number of background counts collected over $t_g$). The noise rate was experimentally determined for our PMT. For a given S/N ratio and number of background counts, the number of signal counts ($N_s$) required is found by solving (10) iteratively for $N_s$. To obtain a statistically significant result for the given S/N ratio, $N_s$ must be larger than the variance, here it is the square root of the total number of counts

$$N_s > \sqrt{N_s + N_b}\,. \quad (11)$$

To find the minimum number of $N_{n+}$ required for detection, (11) is substituted into (6), also recalling that (9a) and (9b) are equal to $N_s$, and then solved for $N_{n+}$ to give (12):

$$N_{n+} > \frac{\sqrt{N_s + N_b}}{\Phi\eta f_{ex} N_{sh}\left[\left(1 - exp^{(-t_g/\tau)}\right) + (t_p/\tau)\right]}. \quad (12)$$

Table 3 gives the optimum value of $t_g$ as a function of lifetime (the point where we are more likely to collect noise rather than a signal photon) along with the LOD for excited electronic state lifetimes over several orders of magnitude from 5 to 1 x $10^5$ ns. The sensitivity calculation was performed over such a large range because the lifetime of any electronically excited states is not known. As the lifetime increases, the sensitivity decreases. This is because a larger value of $t_g$ is required to collect a significant number of signal counts, but a larger time-gate also results in more noise collected. The sensitivity varies by about only one order of magnitude between the shortest and the longest lifetimes on Table 3.

***Table 3.*** *Detection limit for $Th^{n+}$ $n < 4$ ions as a function of $\tau$ and the optimum value for $t_g$.*

| $\tau$ (ns) | $t_g$ (x*$\tau$) | $N_{n+}$ x $10^5$ |
|---|---|---|
| 5 x $10^0$ | 4.7 | 1.0 |
| 1 x $10^1$ | 4.5 | 1.4 |
| 5 x $10^1$ | 3.5 | 2.3 |
| 1 x $10^2$ | 3.1 | 2.6 |
| 5 x $10^2$ | 2.3 | 3.3 |
| 1 x $10^3$ | 2.0 | 3.8 |
| 5 x $10^3$ | 1.6 | 6.0 |
| 1 x $10^4$ | 1.5 | 7.7 |
| 5 x $10^4$ | 1.4 | 15 |
| 1 x $10^5$ | 1.3 | 20 |

The values for $N_{n+}$ in Table 3 assumes that only detector noise is present, but this is not the case in our study. We observed a short-lived background fluorescence. One way to deal with the background fluorescence is to simply remove it by introducing a small delay in the time-gate after the excitation pulse. In our study, the background fluorescence has almost entirely decayed by 150 ns. Removing the signal photons collected during the laser pulse (i.e. $N_{pump}$) and the first 100 ns, it was found that even for lifetimes as short as 50 ns, the calculated sensitivity decreased by only one order of magnitude and the decrease is much less for longer lifetimes. For $\tau$ < 50 ns nearly all of the signal photons would occur during the pump pulse and lifetime of the background fluorescence. Here we estimated the photon rate from the background fluorescence by collecting emission from an annealed $^{229}$Th implanted plate. In order to get an accurate temporal profile and upper estimate on the photon rate, the slits on the monochromator were opened to 1.25 mm and it was tuned to the maximum in the emission spectrum (see Figure 6). Even under these conditions the background fluorescence is relatively weak, and including the additional noise into our sensitivity calculation decreases it by only about an order of magnitude for short (<50 ns) lifetimes.

Our estimate for the LOD is 4-5 orders of magnitude smaller than the total number of implanted $^{229}$Th recoils (2.2 x $10^{10}$). This gives us a wide margin for the error in our estimate for the detection limit. It could be off by a factor of 10,000 and still the upper limit on the number of possible thorium ions in charge states less than 4+ would be small compared to the total number of implanted recoils. We conclude that if $Th^{n+}$ n < 4 ions are present in the $MgF_2$ plate, the number of them are insignificant compared to the total number of implanted $^{229}$Th atoms.

# 6. Conclusion

In this study, we have spectroscopically and theoretically characterized $^{229}$Th implanted $MgF_2$ plates using TRPL, γ-ray spectroscopy and DFT calculations. Our DFT calculations showed that the band gap for $Th^{4+}$ doped $MgF_2$ crystal (11.6 eV) is larger than the energy of the isomeric state (7.8 eV), and our spectroscopic study has shown that the vast majority of the implanted Th ions are present as $Th^{4+}$. Therefore, non-radiative deexcitation of the isomeric state via the internal conversion pathway should be closed in a Th doped $MgF_2$ crystal, making the solid-state approach a promising route towards further development of a nuclear clock.

# Acknowledgements

We thank Audrey Roman for help in collecting the γ-ray spectrum, Joel D. Kress for useful discussion on the chemical potential and crystal chemistry, and John M. Berg for advice on the collection of emission spectra. This work is supported by the Laboratory Directed Research and Development program at Los Alamos National Laboratory, under contract number DE-AC5206NA25396, which is managed and operated by the Los Alamos National Security, LLC for the National Nuclear Security Agency (NNSA) as part of the U.S. Department of Energy.

# References

[1] L. A. Kroger and C. W. Reich, Features of the low-energy level scheme of $^{229}$Th as observed in the α-decay of $^{233}$U, Nucl. Phys. A259, 29 (1976).

[2] R. G. Helmer and C. W. Reich, An excited state of $^{229}$Th at 3.5 eV, Phys. Rev. C 49, 1845 (1994).

[3] C. J. Campbell, A. G. Radnaev, A. Kuzmich, V. A. Dzuba, V. V. Flambaum, and A. Derevianko, Single-ion nuclear clock for metrology at the 19th decimal place, Phys. Rev. Lett. 108, 120802 (2012).

[4] G. A. Kazakov, A. N. Litvinov, V. I. Romanenko, L. P. Yatsenko, A. V. Romanenko, M. Schreitl, G. Winkler, and T. Schumm, Performance of a $^{229}$Thorium solid-state nuclear clock, New J. Phys. 14, 083019 (2012).

[5] T. L. Nicholson, S. L. Campbell, R. B. Hutson, G. E. Marti, B. J. Bloom, R. L. McNally, W. Zhang, M. D. Barrett, M. S. Safronova, G. F. Strouse, W. L. Tew, and J. Ye, Systematic evaluation of an atomic clock at 2 x $10^{-18}$ total uncertainty, Nat. Commun. 6, 6896 (2015).

[6] J. C. Berengut, V. A. Dzuba, V. V. Flambaum, and S. G. Porsev, Proposed experimental method to determine α sensitivity of splitting between ground and 7.6 eV isomeric states in $^{229}$Th, Phys. Rev. Lett. 102, 210801 (2009).

[7] E. Litvinova, H. Feldmeier, J. Dobaczewski, and V. Flambaum, Nuclear structure of lowest $^{229}$Th states and time-dependent fundamental constants, Phys. Rev. C 79, 034302 (2009).

[8] E. V. Tkalya, Proposal for a nuclear gamma-ray laser of optical range, Phys. Rev. Lett. 106, 162501 (2011).

[9] E. Peik and M. Okhapkin, Nuclear clocks based on resonant excitation of γ-transitions, C. R. Phys. 16, 516 (2015).

[10] B. R. Beck, J. A. Becker, P. Beiersdorfer, G. V. Brown, K. J. Moody, J. B. Wilhelmy, F. S. Porter, C. A. Kilbourne, and R. L. Kelley, Energy splitting of the ground-state doublet in the nucleus $^{229}$Th, Phys. Rev. Lett. 98, 142501 (2007).

[11] B. R. Beck, J. A. Becker, P. Beiersdorfer, G. V. Brown, K. J. Moody, C. Y. Wu, J. B. Wilhelmy, F. S. Porter, C. A. Kilbourne, and R. L. Kelley, Improved value for the energy splitting of the ground-state doublet in the nucleus $^{229}$Th in *12th International Conference on Nuclear Reaction Mechanisms*, edited by F. Cerutti, and A. Ferrari (CERN, Genva, 2009), p. 225.

[12] L. von der Wense, B. Seiferle, M. Laatiaoui, J. B. Neumayr, H.-J. Maier, H.-F. Wirth, C. Mokry, J. Runke, K. Eberhardt, C. E. Düllmann, N. G. Trautmann, and P. G. Thirolf, Direct detection of the $^{229}$Th nuclear clock transition, Nature 533, 47 (2016).

[13] W. G. Rellergert, D. DeMille, R. R. Greco, M. P. Hehlen, J. R. Torgerson, and E. R. Hudson, Constraining the evolution of the fundamental constants with a solid-state optical frequency reference based on the $^{229}$Th nucleus, Phys. Rev. Lett. 104, 200802 (2010).

[14] W. G. Rellergert, S. T. Sullivan, D. DeMille, R. R. Greco, M. P. Hehlen, R. A. Jackson, J. R. Torgerson, and E. R. Hudson, Progress towards fabrication of $^{229}$Th-doped high energy band-gap crystals for use as a solid-state optical frequency reference, IOP Conf. Ser.: Mater. Sci. Eng. 15, 012005 (2010).

[15] M. P. Hehlen, R. R. Greco, W. G. Rellergert, S. T. Sullivan, D. DeMille, R. A. Jackson, E. R. Hudson, and J. R. Torgerson, Optical spectroscopy of an atomic nucleus: Progress toward direct observation of the $^{229}$Th isomer transition, J. Lumin. 133, 91 (2013).

[16] X. Zhao, Y. N. Martinez de Escobar, R. Rundberg, E. M. Bond, A. Moody, and D. J. Vieira, Observation of the deexcitation of the $^{229m}$Th nuclear isomer, Phys. Rev. Lett. 109, 160801 (2012).

[17] E. Peik and K. Zimmermann, Comment on "observation of the deexcitation of the $^{229m}$Th nuclear isomer", Phys. Rev. Lett. 111, 018901 (2013).

[18] A. Yamaguchi, M. Kolbe, H. Kaser, T. Reichel, A. Gottwald, and E. Peik, Experimental search for the low-energy nuclear transition in $^{229}$Th with undulator radiation, New J. Phys. 17, 053053 (2015).

[19] J. Jeet, C. Schneider, S. T. Sullivan, W. G. Rellergert, S. Mirzadeh, A. Cassanho, H. P. Jenssen, E. V. Tkalya, and E. R. Hudson, Results of a direct search using synchrotron radiation for the low-energy $^{229}$Th nuclear isomeric transition, Phys. Rev. Lett. 114, 253001 (2015).

[20] E. V. Tkalya, C. Schneider, J. Jeet, and E. R. Hudson, Radiative lifetime and energy of the low-energy isomeric level in $^{229}$Th, Phys. Rev. C 92, 054324 (2015).

[21] J. R. Walensky, R. L. Martin, J. W. Ziller, and W. J. Evans, Importance of energy level matching for bonding in $Th^{3+}$-$Am^{3+}$ actinide metallocene amidinates, $(C_5Me_5)_2[^iPrNC(Me)N^iPr]An$, Inorg. Chem. 49, 10007 (2010).

[22] P. V. Borisyuk, O. S. Vasilyev, A. V. Krasavin, Y. Y. Lebedinskii, V. I. Troyan, and E. V. Tkalya, Band structure and decay channels of thorium-229 low-lying isomeric state for ensemble of thorium atoms adsorbed on calcium fluoride, Phys. Status Solidi C 12, 1333 (2015).

[23] L. von der Wense, P. G. Thirolf, D. Kalb, and M. Laatiaoui, Towards a direct transition energy measurement of the lowest nuclear excitation in $^{229}$Th, JINST 8, P03005 (2013).

[24] L. von der Wense, B. Seiferle, M. Laatiaoui, and P. G. Thirolf, Determination of the extraction efficiency for $^{233}$U source α-recoil ions from the MLL buffer-gas stopping cell, Eur. Phys. J. A 51, 29 (2015).

[25] G. Kresse and J. Hafner, *Ab initio* molecular dynamics for liquid metals, Phys. Rev. B 47, 558 (1993).

[26] G. Kresse and J. Hafner, *Ab initio* molecular-dynamics simulation of the liquid-metal–amorphous-semiconductor transition in germanium, Phys. Rev. B 49, 14251 (1994).

[27] G. Kresse and J. Furthmüller, Efficiency of ab-initio total energy calculations for metals and semiconductors using a plane-wave basis set, Comput. Mat. Sci. 6, 15 (1996).

[28] G. Kresse and J. Furthmüller, Efficient iterative schemes for *ab initio* total-energy calculations using a plane-wave basis set, Phys. Rev. B 54, 11169 (1996).

[29] J. P. Perdew and A. Zunger, Self-interaction correction to density-functional approximations for many-electron systems, Phys. Rev. B 23, 5048 (1981).

[30] P. Dessovic, P. Mohn, R. A. Jackson, G. Winkler, M. Schreitl, G. Kazakov, and T. Schumm, $^{229}$Thorium-doped calcium fluoride for nuclear laser spectroscopy, J. Phys.: Condens. Matter 26, 105402 (2014).

[31] L. Hedin, New method for calculating the one-particle green's function with application to the electron-gas problem, Phys. Rev. 139, A796 (1965).

[32] M. Shishkin and G. Kresse, Implementation and performance of the frequency-dependent GW method within the PAW framework, Phys. Rev. B 74, 035101 (2006).

[33] W. Chen and A. Pasquarello, Band-edge levels in semiconductors and insulators: Hybrid density functional theory versus many-body perturbation theory, Phys. Rev. B 86, 035134 (2012).

[34] A. A. Mostofi, J. R. Yates, G. Pizzi, Y.-S. Lee, I. Souza, D. Vanderbilt, and N. Marzari, An updated version of wannier90: A tool for obtaining maximally-localised Wannier functions, Comput. Phys. Commun. 185, 2309 (2014).

[35] J. Thomas, G. Stephan, J. C. Lemonnier, M. Nisar, and S. Robin, Optical anisotropy of $MgF_2$ in its UV absorption region, Phys. Status Solidi B 56, 163 (1973).

[36] M. Scrocco, Electron-energy-loss and x-ray photoelectron spectra of $MgF_2$, Phys. Rev. B 33, 7228 (1986).

[37] Z. Varga, A. Nicholl, and K. Mayer, Determination of the $^{229}$Th half-life, Phys. Rev. C 89, 064310 (2014).

[38] M. P. Wilkerson and J. M. Berg, Excitation spectra of near-infrared photoluminescence from Np (VI) in $Cs_2U$ (Np) $O_2Cl_4$, Radiochim. Acta 97, 223 (2009).

[39] B. J. Barker, J. M. Berg, S. A. Kozimor, N. R. Wozniak, and M. P. Wilkerson, Visible and near-infrared excitation spectra from the neptunyl ion doped into a uranyl tetrachloride lattice, J. Mol. Struct. 1108, 594 (2016).

[40] S. Y. E. Chu, L. P. Ekstrom, and R. B. Firestone, in *WWW Table of Radioactive Isotopes database version 1999-02-28 URL http://nucleardata.nuclear.lu.se/nucleardata/toi/*2016).

[41] J. G. Solé, L. E. Bausá, and D. Jaque, Applications: Rare Earth and Transition Metal Ions, and Color Centers in *An Introduction to the Optical Spectroscopy of Inorganic Solids* (John Wiley & Sons, Ltd, 2005), p. 207.

[42] J.-C. G. Bunzli and S. V. Eliseeva, Basics of Lanthanide Photophysics in *Lanthanide Luminescence: Photophysical, Analytical and Biological Aspects*, edited by P. Hanninen, and H. Harma (Springer-Verlag, Berlin, 2011), p. 18.

[43] L. Andrews, K. S. Thanthiriwatte, X. Wang, and D. A. Dixon, Thorium Fluorides ThF, $ThF_2$, $ThF_3$, $ThF_4$, $ThF_3(F_2)$, and $ThF_5^-$ Characterized by Infrared Spectra in Solid Argon and Electronic Structure and Vibrational Frequency Calculations, Inorg. Chem. 52, 8228 (2013).

[44] S. P. S. Porto, P. A. Fleury, and T. C. Damen, Raman Spectra of $TiO_2$, $MgF_2$, $ZnF_2$, $FeF_2$ and $MnF_2$, Phys. Rev. 154, 522 (1967).

[45] A. S. Barker, Transverse and Longitudinal Optic Mode Study in $MgF_2$ and $ZnF_2$, Phys. Rev. 136, A1290 (1964).

[46] G. D. Boyd, R. J. Collins, S. P. S. Porto, A. Yariv, and W. A. Hargreaves, Excitation, Relaxation, and Continuous Maser Action in the 2.613-Micron Transition of $CaF_2:U^{3+}$, Phys. Rev. Lett. 8, 269 (1962).

[47] G. J. Quarles, Rare-earth Ions - Miscellaneous: $Ce^{3+}$, $U^{3+}$, divalent, etc in *Handbook of Laser Technology*, edited by C. E. Webb, and J. D. C. Jones (Institute of Physics Publishing, Bristol, 2003), p. 418.

[48] D. F. Shriver and P. W. Atkins, *Inorganic Chemistry 3rd. Edition* (W. H. Freeman and Co., New York, 1999), p. 453.